

# Phase structure, piezoelectric properties, and stability of new $\text{K}_{0.48}\text{Na}_{0.52}\text{NbO}_3\text{--Bi}_{0.5}\text{Ag}_{0.5}\text{ZrO}_3$ lead-free ceramics

Xiaopeng Wang · Jiagang Wu · Xiang Lv ·  
Hong Tao · Xiaojing Cheng · Ting Zheng ·  
Binyu Zhang · Dingquan Xiao · Jianguo Zhu

Received: 16 April 2014 / Accepted: 10 May 2014 / Published online: 18 May 2014  
© Springer Science+Business Media New York 2014

**Abstract** In this work,  $(1-x)(\text{K}_{0.48}\text{Na}_{0.52})\text{NbO}_3\text{--}x(\text{Bi}_{0.5}\text{Ag}_{0.5})\text{ZrO}_3$  [(1-x)KNN-xBAZ] lead-free piezoceramics was prepared by the conventional solid-state method, and a new phase boundary consisting of three phases [e.g., rhombohedral, orthorhombic, and tetragonal (R–O–T) phases] has been constructed by adding both  $(\text{Bi}_{0.5}\text{Ag}_{0.5})^{2+}$  and  $\text{Zr}^{4+}$ . The ceramic with  $x = 0.05$  possesses an R–O–T phase coexistence. A large  $d_{33}$  of  $\sim 347$  pC/N and a high  $T_C$  of  $\sim 318$  °C have been shown in the ceramic with  $x = 0.05$ . In addition, such a ceramic also possesses enhanced thermal and temperature stability of piezoelectricity and ferroelectricity. Both the phase boundary and the grain size play a critical role in large piezoelectricity and good stability. We think that this material belongs to be one of the promising candidates for the high-temperature piezoelectric devices.

## 1 Introduction

Lead-based ceramics widely used in some electronic devices are harmful to the environmental and human health during their processing and applications [1, 2]. So, it is urgent to find one kind of new lead-free piezoceramics for replacing lead-based ones. Over the past years, the perovskite-type lead-free piezoceramics have attracted much attention because of their good electrical properties [3–10, 12, 13, 15–25], such as  $(\text{K},\text{Na})\text{NbO}_3$  [4–13, 15–19, 21–25],  $(\text{Bi}_{0.5}\text{Na}_{0.5})\text{TiO}_3$  [3], and  $\text{BaTiO}_3$  [20].

In 2004, Satio et al. [4] reported a new ceramics based on Li, Ta, and Sb-modified KNN with a giant piezoelectric constant ( $d_{33}$ ) 416 pC/N by the reactive-templated grain growth, and since then, KNN ceramics have intrigued the enthusiasm of most researchers [5–10, 12, 13, 15–25]. In order to further enhance piezoelectric properties of KNN-based ceramics, lots of attention has been given to the design of their phase boundaries by finely tailoring its compositions [5–7, 9, 10, 12, 18]. Recently, we have reported new material systems consisting of KNN by constructing the R-T phase boundary, and a giant  $d_{33} \sim 490$  pC/N has been attained by tailoring their compositions [5]. However, those material systems containing Sb may be also harmful to the human health during their processing because of its light toxicity, and adding  $\text{Sb}^{5+}$  could also drop the curie temperature ( $T_c$ ) rapidly and result in a relatively poor temperature stability of the KNN, limiting their practical applications [5–7, 9, 12, 22, 24, 25]. So, it is urgent to find some new material systems with a large piezoelectricity and good temperature stability in the road of replacing lead-based ones.

In this work,  $(1-x)(\text{K}_{0.48}\text{Na}_{0.52})\text{NbO}_3\text{--}x(\text{Bi}_{0.5}\text{Ag}_{0.5})\text{ZrO}_3$  [(1-x)KNN-xBAZ] lead-free piezoceramics were prepared by the conventional solid-state method. Here, the addition of both  $(\text{Bi}_{0.5}\text{Ag}_{0.5})^{2+}$  and  $\text{Zr}^{4+}$  not only modifies the phase transition temperature (i.e.,  $T_{\text{O-T}}$  and  $T_{\text{R-O}}$ ) but also changes the grain size of the ceramics. Finally, a phase boundary consisting of rhombohedral, orthorhombic, and tetragonal phases (R–O–T) could be found in the compositions of around  $x = 0.05$ , and a dense structure could be also detected. In addition, the underlying physical mechanisms for composition-induced phase boundary and the relationship between grain size and electrical properties were importantly addressed.

X. Wang · J. Wu (✉) · X. Lv · H. Tao · X. Cheng ·  
T. Zheng · B. Zhang · D. Xiao · J. Zhu  
Department of Materials Science, Sichuan University,  
Chengdu 610064, People's Republic of China  
e-mail: wujiagang0208@163.com; msewujg@scu.edu.cn

## 2 Experimental procedure

$(1-x)(\text{K}_{0.48}\text{Na}_{0.52})\text{NbO}_3-x(\text{Bi}_{0.5}\text{Ag}_{0.5})\text{ZrO}_3$  lead-free piezoceramics were prepared by the conventional mixed oxide method.  $\text{Na}_2\text{CO}_3$  (99.8 %),  $\text{K}_2\text{CO}_3$  (99.0 %),  $\text{Nb}_2\text{O}_5$  (99.5 %),  $\text{ZrO}_2$  (99.0 %),  $\text{Ag}_2\text{O}$  (99 %), and  $\text{Bi}_2\text{O}_3$  (99.999 %) were used as starting raw materials, and ball milled for 24 h with agate ball media and alcohol. After calcination at 850 °C for 6 h, these powders were pressed into disks of  $\sim 1.0$  cm diameter and  $\sim 1.0$  mm thickness at 10 MPa using PVA as a binder. After burning off PVA, the green pellets with  $x = 0, 0.02, 0.03, 0.04, 0.045, 0.05, 0.055, 0.06,$  and  $0.07$  were sintered at 1,070, 1,070, 1,070, 1,080, 1,080, 1,080, 1,090, 1,090, and 1,090 °C, respectively. The silver paste was fired on both sides of the samples at 700 °C for 10 min to form the electrodes for electrical measurements. These samples were poled in a silicon oil bath under different temperature by applying a direct current electric field of 3–4 kV/mm for 15 min.

X-ray diffraction (XRD) characterization of these sintered samples was performed using  $\text{Cu } k_\alpha$  radiation in the  $\theta$ - $2\theta$  scan mode (Bruker D8 Advanced XRD, Bruker AXS Inc., Madison, WI, CuK $\alpha$ ). Their microstructure (i.e., surface and cross section) and element mapping were measured and recorded by a field-emission scanning electron microscope (FE-SEM) (JSM-7500, Japan). The capacitance and dissipation factors of the sintered samples were measured using a programmable furnace with an LCR analyzer (HP 4980, Agilent, USA) with a varied temperature  $-150$ – $200$ , and  $30$ – $450$  °C. The  $d_{33}$  value was measured using a piezo- $d_{33}$  meter (ZJ-3A, China). The planar electromechanical coupling factor  $k_p$  were measured by using an impedance analyzer (HP 4294A). The polarization versus electric field ( $P$ - $E$ ) hysteresis loops of the unpoled cylindrical pellets were measured at 10 Hz with a ferroelectric tester (radiant Technologies, Inc. Albuquerque, NM, USA).

## 3 Results and discussion

As shown in Fig. 1a, the XRD patterns of  $(1-x)\text{KNN}-x\text{BAZ}$  ceramics as a function of BAZ content were measured at room temperature, and it can be found that all the ceramics show a typical perovskite structure, and no second phases were found. These results indicated that both  $(\text{Bi}_{0.5}\text{Ag}_{0.5})^{2+}$  and  $\text{Zr}^{4+}$  have completely diffused into the KNN matrix forming a new solid solution. The expanded XRD analysis was made in the range of  $2\theta = 43^\circ$ – $48^\circ$ , as shown in Fig. 1b. It could be observed that all the ceramics showed different peak shapes, dependent on the BAZ content, and it can be only affirmed that the pure KNN owns an orthorhombic phase [9–11, 17, 19, 24]. The capacitance of  $(1-x)\text{KNN}-$

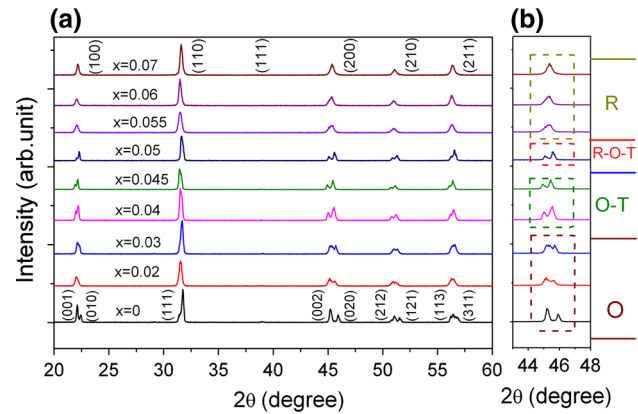


**Fig. 1** a XRD patterns and b expanded XRD patterns of  $(1-x)\text{KNN}-x\text{BAZ}$  ceramics as a function of BAZ content

$x\text{BAZ}$  ceramics with  $x = 0.02, 0.03, 0.04, 0.045, 0.05, 0.055,$  and  $0.06$  were measured at 10 kHz and in the temperature from  $-150$  to  $200$  °C in order to analyze the evolution of the phase structure of ceramics deeply, as seen in Fig. 2. It could be found that, with the increase of BAZ content, the  $T_{\text{O-T}}$  is shifted to a lower temperature, while the peak of  $T_{\text{R-O}}$  phase boundary almost keeps unchanged and becomes broader, and even disappears when  $x = 0.05$ . Figure 3 plots the temperature dependence of the dielectric constant of the ceramics, measured at 10 kHz. As seen in Fig. 3, the dielectric peak ( $T_C$ ) slightly changes from 358 to 320 °C with the increase of BAZ content ( $x \leq 0.05$ ), and the maximum dielectric constant located at  $T_C$  reaches maximum when  $x = 0.05$  because of the involved phase boundary. In addition, the  $\epsilon_r$ - $T$  curves become broadened for the ceramics with  $x \geq 0.055$  owing to the dramatic decrease in grain size [20]. Figure 4 showed the phase diagram of the  $(1-x)\text{KNN}-x\text{BAZ}$  ceramics determined by the XRD patterns and  $\epsilon_r$ - $T$  curves. It could be found in Fig. 4 that both the  $T_{\text{O-T}}$  and  $T_C$  are very sensitive to the changes of their composition, while the  $T_{\text{R-O}}$  almost keeps the same. In this material system, the addition of the BAZ content could shift the peak of  $T_{\text{O-T}}$  close to the room temperature, and “weakened” the peak of the phase transition from rhombohedral to orthorhombic phase, or that the rhombohedral and orthorhombic phase coexistence range become border. Thus, a new phase boundary consisting of rhombohedral, orthorhombic and tetragonal phases could be constructed around the composition of  $x = 0.05$  in the room temperature. In addition, a high  $T_C$  of about 318 °C could be found in the composition of  $x = 0.05$  in this work. Both an excellent  $d_{33}$  and a higher  $T_C$  mean that this kind of ceramics could be more easily used in the practical applications, especially for high-temperature applications.

In  $\text{Pb}(\text{Zr},\text{Ti})\text{O}_3$  and  $\text{BaTiO}_3$  ceramics, the grain size plays an important in the enhancement in electric properties [11, 14, 20], and it was reported that the grain size of KNN also

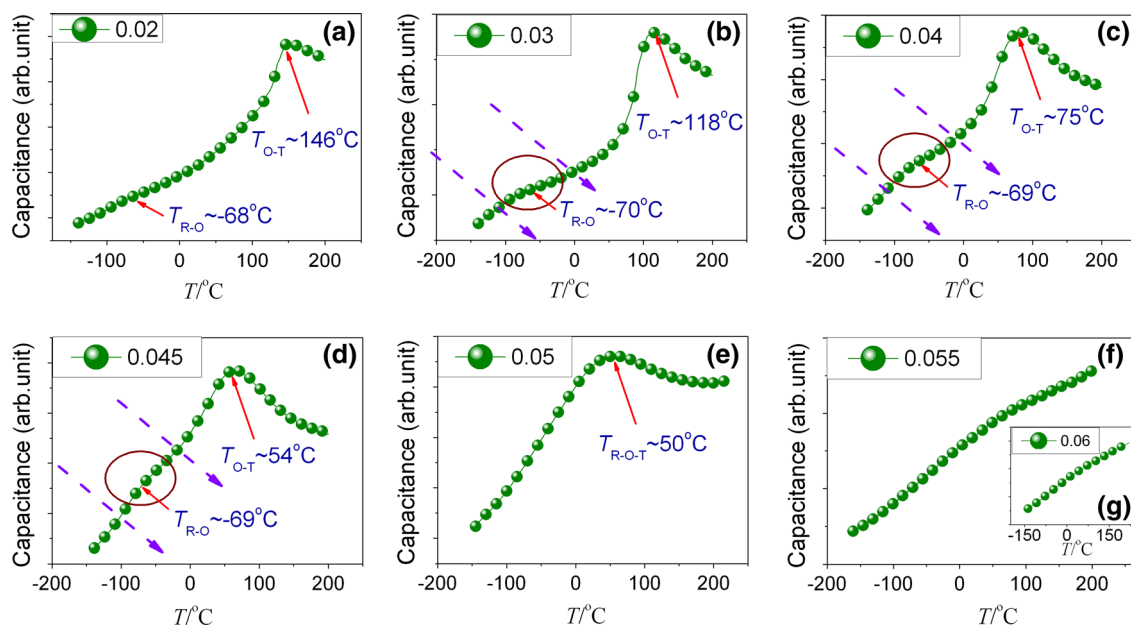


**Fig. 2** Capacitance of  $(1 - x)\text{KNN}-x\text{BAZ}$  ceramics in the temperature from 220 to  $-150$  °C, measured at 10 kHz: **a**  $x = 0.02$ , **b** 0.03, **c** 0.04, **d** 0.045, **e** 0.05, **f** 0.055, and **g** 0.06

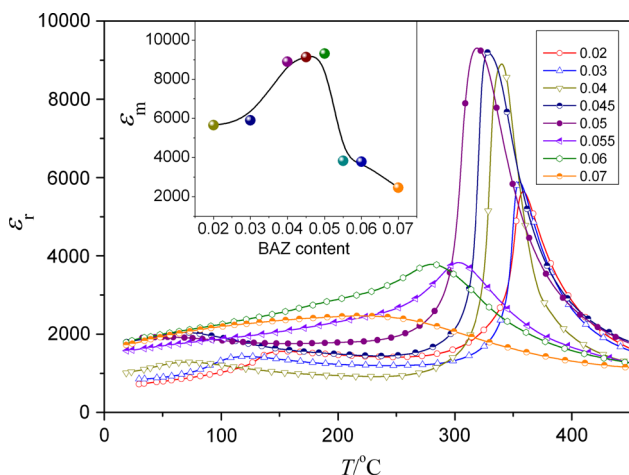


**Fig. 3** Temperature dependence of dielectric constant of  $(1 - x)\text{KNN}-x\text{BAZ}$  ceramics as a function of BAZ content. The inset shows the peak of the  $T_C$  changed as a function of BAZ content

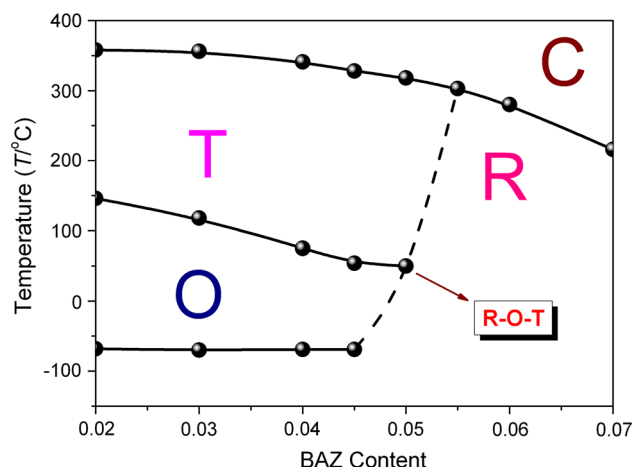


**Fig. 4** Phase diagram of the  $(1 - x)\text{KNN}-x\text{BAZ}$  ceramics

has a very close relationship with the stability of the ceramics [8, 24, 25]. Figures 5a–b showed the SEM images of the surface microstructure deriving from the  $(1 - x)\text{KNN}-x\text{BAZ}$  ceramics. As shown in Fig. 5, the grain size first dropped, then increased (reaching the maximum at  $x = 0.05$ ), and at last became much smaller with further increasing BAZ content. The decrease in grain size may be caused by the limit of the Zr element with the addition of the BAZ [12]. In addition, it can be also found that the ceramics with  $x = 0, 0.03$ , and  $0.06$  show a more loose structure, while the ceramics with  $x = 0.05$  possess a denser structure

without observable pores. Generally speaking, the domain variants were likely to be limited, and the density of the domain was relatively increased with the decrease of the grain size, which would make the saturation polarization more difficult and have a negative influence on the piezoelectric properties and the stability of the ceramics [8, 11, 14]. In addition, the decrease of the grain size also “strengthened” the coupling between grain boundaries and domain walls, which would make the reorientation more difficult and constrain the domain wall motion in some content [8, 11]. Therefore, this may be a significant reason to the degradation in piezoelectric properties and stability [24, 25]. To avoid the deviation of the surface microscopy caused



**Fig. 5** SEM patterns of the surface (1- $x$ )KNN- $x$ BAZ ceramics with **a**  $x = 0$ , **b**  $x = 0.03$ , **c**  $x = 0.05$ , **d**  $x = 0.06$

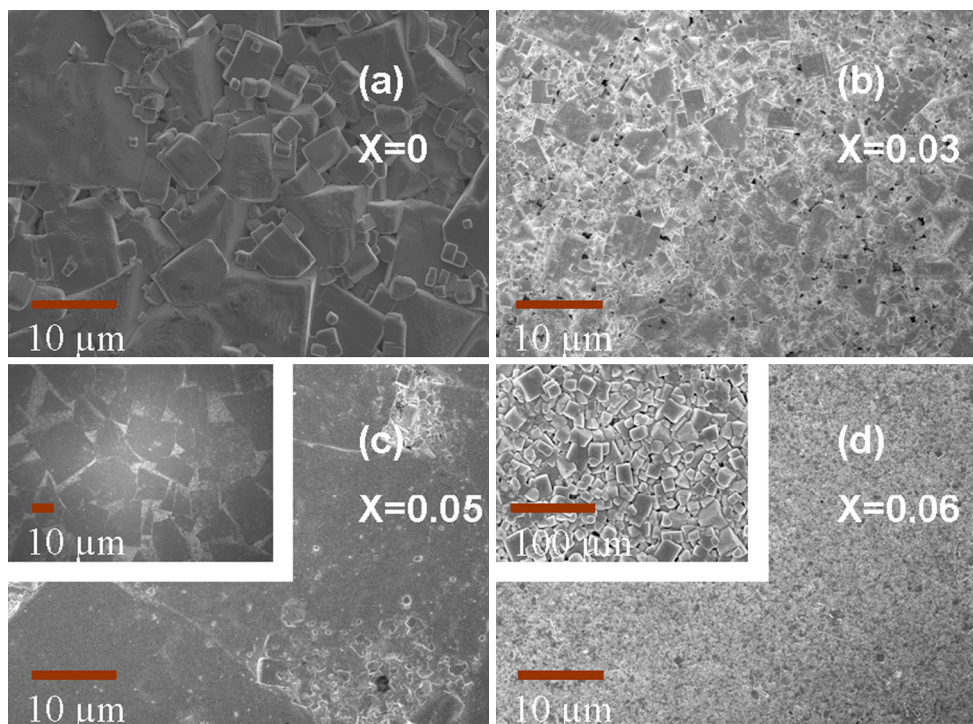
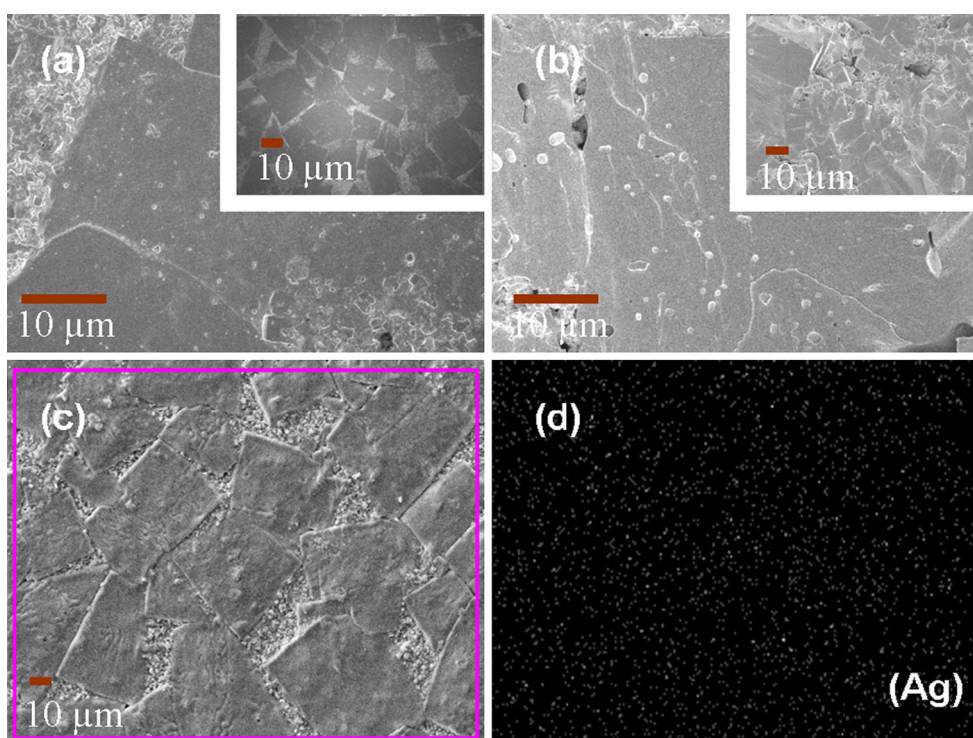


**Fig. 6** SEM patterns of the surface **(a)** and fracture surface **(b)** of 0.95KNN-0.05BAZ ceramics; **(c, d)** Elemental mapping of the 0.95KNN-0.05BAZ ceramics



by the volatilization of the element or other factors, the SEM image of its fracture was also done, as shown in Fig. 6b. It can be seen that, similarity to its surface, the interface also presents the similar grain size and owns a relative dense structure. For further analyzing the distribution of Ag in the

ceramic matrix, the element mapping of Ag was made in Fig. 6d. As shown in Fig. 6c and d, one can see that the Ag is homogeneously distributed in the whole ceramics.

Herbiet et al. [26] believe that the electric properties are dependent on the intrinsic and extrinsic portions and it could

be by simply expressing the physical properties in terms of sum:  $\varepsilon = \varepsilon_{\text{ex}} + \varepsilon_{\text{in}}$ ;  $d = d_{\text{ex}} + d_{\text{in}}$ : where  $\varepsilon$  stands for the dielectric permittivity,  $d$  the piezoelectric coefficient. Figure 7a plotted the  $\varepsilon_r$  and  $\tan \delta$  values of  $(1-x)\text{KNN}-x\text{BAZ}$  ceramics measured at 10 kHz. As shown in Fig. 7a, the  $\varepsilon_r$  value of the ceramics increased with the increase of BAZ content ( $x < 0.05$ ), became flat for  $0.05 \leq x \leq 0.06$ , and finally dropped for  $x > 0.06$ . The trend of the permittivity could be explained by two aspects (e.g., the intrinsic and extrinsic factors), and both the phase structure and the grain size had a critical effect on the dielectric constant [26]. Unlike the  $\varepsilon_r$  values, the curves of the  $\tan \delta$  presented another trend. The  $\tan \delta$  values of these ceramics fluctuate with the increase of the BAZ content, reaching minimum ( $\sim 3.3\%$ ) for the ceramic with  $x = 0.05$ . Interestingly, the varying of the dielectric loss presented the opposite trends to the grain size. Both Herbiet and Damjanovic thought that the extrinsic contribution was related to the dielectric loss [26, 27]. With the decrease of grain size, the density of the domains increased, the domain wall mobility decreased, and the strength between the domain wall and the grain boundaries increased, finally leading to the increase of the  $\tan \delta$  value. Figure 7b showed the  $P-E$  hysteresis loops of the ceramics as a function of  $x$ , measured at 10 Hz and room temperature. As can be seen in Fig. 7b, all the ceramics exhibited a well-saturated hysteresis loop. In addition, it could be shown in Fig. 7c that the remanent polarization ( $P_r$ ) presented the trend of increase with the increase of BAZ, reaching a maximum when  $x = 0.05$ . Enhanced ferroelectric properties should be assigned to the coexistence of the R-O-T phases and the increase of the grain size. At the same time, the coercive field ( $E_c$ ) changes slightly with varying BAZ content. Figure 7d showed the  $d_{33}$  and  $k_p$  of the  $(1-x)\text{KNN}-x\text{BAZ}$  ceramics as a function of BAZ content. It could be seen that both the  $d_{33}$  and  $k_p$  almost have the same trend with the increase of BAZ content, that was, reaching the maximum ( $d_{33} \sim 347$  pC/N and  $k_p \sim 48\%$ ) at  $x = 0.05$ . As for the intrinsic structure, the formation of R-O-T phase boundary played an important role in the piezoelectric properties of the ceramics. Generally, it could be found that the relatively large  $d_{33}$  of most KNN systems is related to the construction of the phase boundary, which are assigned to be  $T_{\text{R-O}}$ ,  $T_{\text{O-T}}$ ,  $T_{\text{R-T}}$  and  $T_{\text{R-O-T}}$  [5–7, 9, 10, 12, 18]. In the other hand, the grain size of this work also had significant effects on the piezoelectric properties. With the decrease of the grain size, the domain itself variants was limited, and the coupling strength between the grain boundaries and the domain wall increased, resulting in the lower piezoelectric properties [8, 11, 14]. Therefore, the increase of grain size should be partly attributed to the enhancement in the piezoelectricity. Figure 7e plots the  $d_{33}$  values of the 0.95KNN-0.05BAZ ceramics under different sintering temperatures ( $T_s$ ). As shown in Fig. 7e, the optimum  $T_s$  of this ceramic was

1,080 °C according to the evaluation of their piezoelectricity, and too low  $T_s$  would make this material difficult to turn ceramics, while too high  $T_s$  could result in the deviation of composition in the ceramics, thus worsened the piezoelectric properties of the ceramics [8]. In addition, with the increase of the  $T_s$ , the piezoelectric properties of the ceramics just decreased slightly when  $T_s > 1,080$  °C, showing that the 0.95KNN-0.05BAZ ceramics was easily to be sintered in a wide  $T_s$  of 1,080–1,100 °C. To illuminate the relationship among their ferroelectric, dielectric, and piezoelectric properties, we plotted both  $\varepsilon_r P_r$  and  $d_{33}$  of the  $(1-x)\text{KNN}-x\text{BAZ}$  ceramics as a function of the BAZ content, as shown in Fig. 7f. Generally, a much higher  $\varepsilon_r P_r$  corresponded to a much larger  $d_{33}$ , where  $\varepsilon_r P_r$  was often used to illuminate the physical mechanism for the enhancement in  $d_{33}$  of piezoelectric materials [5, 6, 8, 12]. As shown in Fig. 7f, similarity to the trend of the  $d_{33}$ , the  $\varepsilon_r P_r$  reaches maximum for the ceramics with  $x = 0.05$ , showing that the enhanced dielectric and ferroelectric properties are also responsible for the improved piezoelectricity.

The stability of the piezoceramics was a very important factor for practical applications in electronic devices. And, the thermal-depoling behavior of  $d_{33}$  and temperature-dependent  $P-E$  loops of the ceramics were studied in this work. As shown in Fig. 8a, the ceramics with  $0.03 \leq x \leq 0.05$  kept a rather good thermal stability in a wide range of 30–300 °C. To analysis the stability as a function of the BAZ content accurately, the annealing temperature ( $\Delta d_{33}/d_{33} \sim 20\%$ )  $T_d$  changed with the BAZ content was made in Fig. 8b. As shown in Fig. 8b, with the increase of the BAZ content,  $T_d$  increased, reaching the maximum 310 °C, when  $x = 0.05$ , and then decreased. This result indicated that 0.95KNN-0.05BAZ ceramics possessed a good stability. The good temperature stability may be also caused by the intrinsic and extrinsic factors. In terms of the phase structure, with increasing temperatures, the crystal lattice parameters were easily to be changed, and the tetragonality ( $c/a$ ) decreased rapidly, while the orthorhombic lattice parameters changed little with temperatures, or in other words, the orthorhombic phase presents much better piezoelectric temperature stabilities than in the tetragonal phase [24, 25]. On the other hand, the domain wall mobility and contribution caused by the changes of grain size and phase structure also affected the stability of the piezoelectric properties [8, 14]. The stability of the ferroelectric phase was another aspect to characterize the stability of the ceramics, and it was mainly determined by the additional composition [20]. Figure 8(c) plotted the temperature-dependent  $P-E$  loops of the ceramics with  $x = 0.05$ , measured at 30–180 °C and  $f = 10$  Hz. It could be found that all  $P-E$  loops exhibit similar hysteretic behavior, regardless of the measurement temperatures. In addition, it can be also observed from Fig. 8d, which was obtained from the

**Fig. 7** **a**  $\varepsilon_r$  and  $\tan \delta$  values of  $(1-x)\text{KNN}-x\text{BAZ}$  ceramics measured at 10 kHz; **b, c**  $P$ - $E$  hysteresis loops of the ceramics as a function of  $x$  measured at room temperature at 10 Hz; **d**  $d_{33}$  and  $k_p$  of the ceramics as a function of BAZ content; **e**  $d_{33}$  values of the 0.95KNN-0.05BAZ ceramics in different sintering temperature; **f**  $d_{33}$  and  $\varepsilon_r P_r$  of the ceramics with different BAZ contents

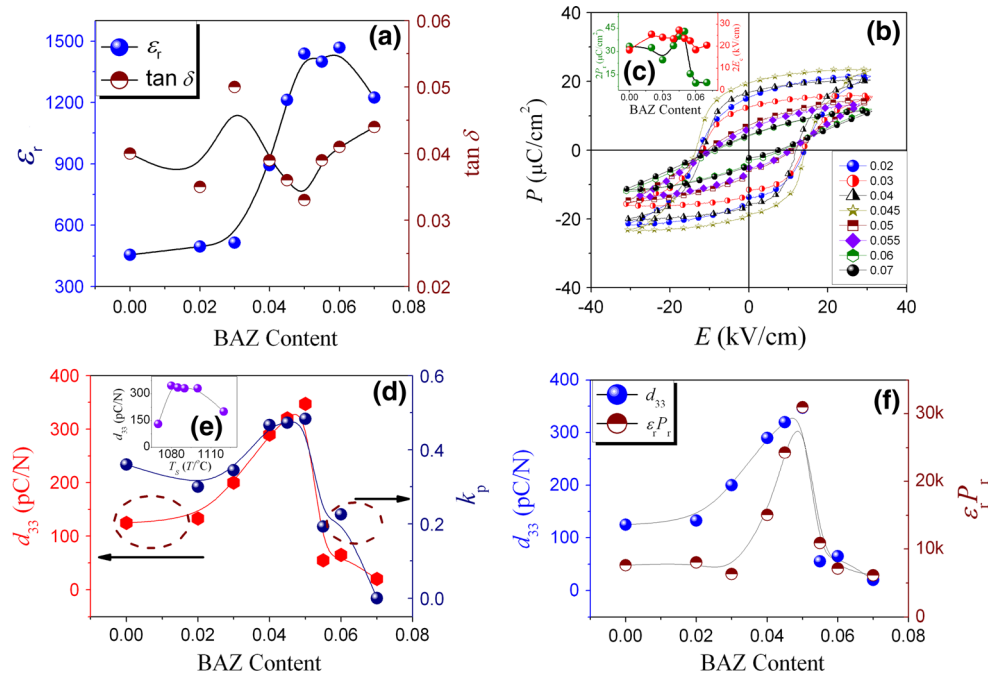
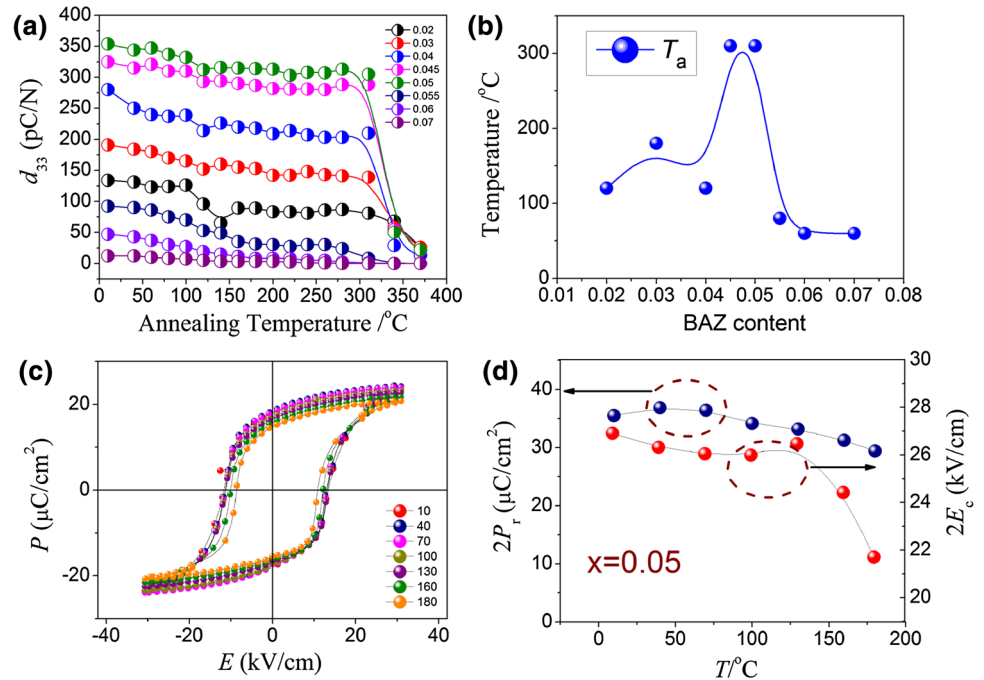


**Fig. 8** **a, b** Thermal-depoling behaviour of  $d_{33}$  and  $k_p$  values of the ceramics; **c**, **d** Temperature-dependence  $P$ - $E$  loops of the 0.95KNN-0.05BAZ ceramics



$P$ - $E$  loops shown in Fig. 8c, the  $P_r$  slightly decreased and the  $E_c$  gradually dropped with the increase of the temperatures. It was noted that the  $P_r$  decreases from 17.74 to 14.71  $\mu\text{C}/\text{cm}^2$  when the measurement temperatures increased from 30  $^\circ\text{C}$  up to 180  $^\circ\text{C}$ , and  $\Delta P_r/P_r(30\text{ }^\circ\text{C})$  was 27 % when the temperature reached 180  $^\circ\text{C}$ , which almost matched the change in thermal stability of  $d_{33}$ . As a result, the ceramic with  $x = 0.05$  showed an improved thermal

stability of piezoelectric properties and an enhanced temperature stability of ferroelectric properties.

#### 4 Conclusions

$(1-x)\text{KNN}-x\text{BAZ}$  lead-free piezoceramics have been prepared by the conventional solid-state method. The



R–O–T phase boundary could be designed and the dense structure with a large grain size could be developed with the addition of BAZ ( $x \sim 0.05$ ), thus their electrical properties could be greatly enhanced. The ceramic with  $x = 0.05$  has a piezoelectric behavior of  $d_{33} \sim 347$  pC/N, together with a high  $T_c \sim 318$  °C. We believe that both the intrinsic and extrinsic factors should be considered in the explanation of the enhanced electrical properties and good temperature stability. The intrinsic properties are mainly dependent on the phase structure, while the relative role of extrinsic contribution is deduced to be influence strongly by the grain size [11]. The doping of BAZ gives an effective way to enhance the electrical properties and temperature stability of the KNN-based ceramics.

**Acknowledgments** Authors gratefully acknowledge the supports of the National Science Foundation of China (NSFC Nos. 51102173, 51272164, and 51332003), the Fundamental Research Funds for the Central Universities (2012SCU04A01), and the introduction of talent start funds of Sichuan University (2082204144033). Thank Ms. Hui Wang for measuring the SEM patterns and beneficial discussions.

## References

1. T. Yamamoto, Jpn. J. Appl. Phys. **35**, 5104–5108 (1996)
2. B. Jaffe, Academic Press, India, Chap. 7. (1971)
3. A. Sasaki, T. Chiba, Y. Mamiya, E. Otsuki, Jpn. J. Appl. Phys. **38**(9B), 5564–5567 (1999)
4. Y. Saito, H. Takao, T. Tani, T. Nonoyama, K. Takatori, T. Homma, T. Nagaya, M. Nakamura, Nature **432**, 84–87 (2004)
5. X.P. Wang, J.G. Wu, D.Q. Xiao, J.G. Zhu, X.J. Cheng, T. Zheng, B.Y. Zhang, X.J. Lou, X.J. Wang, J. Am. Chem. Soc. **136**, 2905–2910 (2014)
6. X.P. Wang, J.G. Wu, D.Q. Xiao, X.J. Cheng, T. Zheng, B.Y. Zhang, X.J. Lou, J.G. Zhu, J. Mater. Chem. A. **2**, 4122–4126 (2014)
7. R.Z. Zuo, J. Fu, J. Am. Ceram. Soc. **94**(5), 1467–1470 (2011)
8. J.G. Wu, X.P. Wang, X.J. Cheng, T. Zheng, B.Y. Zhang, D.Q. Xiao, J.G. Zhu, X.J. Lou, J. Appl. Phys. **115**, 114104 (2014)
9. J.G. Wu, Y.Y. Wang, D.Q. Xiao, J.G. Zhu, P. Yu, L. Wu, W.J. Wu, Jpn. J. Appl. Phys. **46**, 7375–7377 (2007)
10. R.Z. Zuo, X.S. Fang, C. Ye, Appl. Phys. Lett. **90**, 092904 (2007)
11. C.A. Randall, N. Kim, J. Kucera, W.W. Cao, T.R. Shorut, J. Am. Ceram. Soc. **81**(3), 677 (1998)
12. X.P. Wang, J.G. Wu, X.J. Cheng, B.Y. Zhang, D.Q. Xiao, J.G. Zhu, X.J. Wang, X.J. Lou, J. Phys. D Appl. Phys. **46**, 495305 (2013)
13. H. Du, D. Liu, F. Tang, D. Zhu, W. Zhou, J. Am. Ceram. Soc. **90**(9), 2824–2829 (2007)
14. W.W. Gao, C.A. Randall, J. Phys. Chem. Solids **57**, 1499–1505 (1996)
15. J. Rödel, W. Jo, K.T.P. Seifert, E.M. Anton, T. Granzow, D. Damjanovic, J. Am. Ceram. Soc. **92**, 1153–1177 (2009)
16. S.J. Zhang, R. Xia, T.R. Shorut, Appl. Phys. Lett. **9**, 132913 (2007)
17. C. Lei, Z.G. Ye, Appl. Phys. Lett. **93**, 042901 (2008)
18. W. Liang, W. Wu, D. Xiao, J. Zhu, J. Am. Ceram. Soc. **94**(12), 4317 (2011)
19. J. Wu, D. Xiao, Y. Wang, J. Zhu, P. Yu, Y.H. Jiang, J. Appl. Phys. **102**, 114113 (2007)
20. Z. Zhao, V. Buscaglia, M. Viviani, M.T. Buscaglia, L. Mitoseriu, A. Testino, M. Nygren, M. Johnsson, P. Nanini, Physical. Review. B. **70**, 0163–1829 (2004)
21. D.M. Lin, K.W. Kwork, H.L.W. Chan, J. Appl. Phys. **102**, 034102 (2007)
22. J. Du, X. Yi, C. Ban, Z. Xu, P. Zhao, C. Wang, Ceram. Int. **39**, 2135–2139 (2013)
23. T.R. Shorut, S.J. Zhang, J. Electroceram. **19**, 111–124 (2007)
24. Y. Gao, J.L. Zhang, X.J. Zong, C.L. Wang, J.C. Li, J. Appl. Phys. **107**, 074101 (2010)
25. L.M. Zheng, J.F. Wang, Q.Z. Wu, R. Zhang, C.M. Wang, Z.G. Gai, Phys. Status. Solid. A. **208**(4), 915–918 (2010)
26. R. Herbiet, U. Robels, H. Dederichs, G. Arlt, Ferroelectrics **98**, 107–121 (1989)
27. D. Damjanovic, M. Demartin, Appl. Phys. Lett. **68**(21), 3046–3048 (1996)